Exceptional-point-induced lasing dynamics in a non-Hermitian Su-Schrieffer-Heeger model

K. L. Zhang, P. Wang, and Z. Song*
School of Physics, Nankai University, Tianjin 300071, China

(Received 21 August 2018; published 10 April 2019)

Non-Hermitian systems exhibit many peculiar dynamic behaviors that never showed up in Hermitian systems. The existence of spectral singularity for a non-Hermitian scattering center provides a "lasing mechanism" in the context of quantum mechanics. In this paper, we investigate the dynamics of the non-Hermitian Su-Schrieffer-Heeger model around an exceptional point, based on an analysis of parity-time and chiral-time symmetries of the Hamiltonian. We show exactly that a finite system near its exceptional point can support EP-related amplification of cyclic states. It becomes a stationary laser solution with linear-power amplification under certain conditions in an infinite limit. In contrast to the SS lasing mechanism for a scattering system, such an SSH chain acts as an active laser medium at threshold, within which a stationary particle emission can be fired anywhere, rather than a specific location at the non-Hermitian scattering center only. In addition, some relevant peculiar phenomena arising from interference between wave packets are revealed based on the analytical solutions.

DOI: 10.1103/PhysRevA.99.042111

I. INTRODUCTION

Recent developments in non-Hermitian quantum mechanics [1–14] have opened up new research directions in several branches of physics [15–29]. The remarkable features of a non-Hermitian system are the violation of conservation law of the Dirac probability, and the exceptional point (EP) [30–33] or spectral singularity (SS) [34–40]. Based on the former, the complex potential is employed to describe open systems phenomenologically [41]. Furthermore, unconventional propagation of light associated with the gain or loss has been demonstrated by engineering effective non-Hermitian Hamiltonians in optical systems [20,42,43]. On the other hand, many unique optical phenomena have been observed around the EP, ranging from loss-induced transparency [20], power oscillations violating left-right symmetry, low-power optical diodes [25], to single-mode laser [27,28]. A fascinating phenomenon of non-Hermitian optical systems in the application aspect is the gain-induced detection, such as enhanced spontaneous emission [44], enhanced nanoparticle sensing [45], as well as the amplified transmission in the optomechanical system [46,47]. Both theoretical and experimental works not only give insight into the dynamical property of the non-Hermitian Hamiltonian, but they also provide a platform to implement the optical phenomenon.

In this paper, we investigate the lasing mechanism arising from a non-Hermitian system. Based on the novel feature of a non-Hermitian scattering center [36], it is pointed out that an SS can represent lasing with zero linewidth [48]. It has been shown that a Gaussian wave packet can stimulate stationary laser states when it meets the non-Hermitian scattering center [49,50]. By using Fano resonance in a $\mathcal{PT}$-symmetric system with a pair of side-coupled balanced gain and loss resonators, spectral singularity induces unidirectional lasing [51], where spectral singularities exhibit nonreciprocity. In this work, we present another lasing mechanism beyond the scattering problem. We focus on a non-Hermitian system with bulk translational symmetry. For an arbitrary state $\sum_n C_n|\phi_n\rangle$ that consists of a set of eigenstates $|\phi_n\rangle$ with superposition coefficients C_n and real energy E_n, the time evolution of this state has the form $\sum_n C_n e^{-iE_n t}|\phi_n\rangle$. The Dirac probability of $\sum_n C_n e^{-iE_n t}|\phi_n\rangle$ is not conservative but periodic. On the other hand, a coalescing state $|\phi_c\rangle$ at the EP evolves in a special way. Its Dirac probability increases in t^2 [52–54]. It is presumable that when several $|\phi_n\rangle$ approach $|\phi_c\rangle$, a proper superposition of them may exhibit some interesting behavior, e.g., the Dirac probability increases linearly in time in a period of time. It corresponds to a stationary power amplification laser state.

To demonstrate this lasing scheme, we consider a one-dimensional (1D) $\mathcal{PT}$-symmetry non-Hermitian Su-Schrieffer-Heeger (SSH) model [55]. By using the exact solutions, we introduce a mechanism for self-sustained emission in finite non-Hermitian systems at the EP. We show that, without the existence of SS in a scattering system, one is able to obtain a class of stationary EP-related amplification of cyclic states. For such solutions, a lasing mode is fired at any location of the system, which acts as an active lasing medium, rather than the non-Hermitian scattering center only in the context of the SS regime. In addition, it is found that the superposition of these states exhibits some counterintuitive dynamical behaviors. Although the system is noninteracting, a delicate design of the interference process results in the phenomenon of wave-packet–pair annihilation and creation.

The remainder of this paper is organized as follows. In Sec. II, we present a non-Hermitian SSH chain model and the formulation of approximate diagonalization. Section III presents the laser solution and reveals the lasing dynamics for specific initial localized states. In Sec. IV, we consider the physical realization by investigating the evolution of a Gaussian-type initial state. Section V demonstrates some

*songtc@nankai.edu.cn

peculiar dynamical behaviors in the present system. Finally, we give a summary and discussion in Sec. VI.

II. MODEL AND SOLUTION

To begin, we briefly summarize the known properties of the 1D non-Hermitian SSH model with staggered balanced gain and loss. It has been studied systematically in previous work [55,56]. The simplest tight-binding model with these features is

$$H = (1+\delta)\sum_{j=1}^{N} a_j^\dagger b_j + (1-\delta)\sum_{j=1}^{N-1\text{ or }N} b_j^\dagger a_{j+1} + \text{H.c.} + i\gamma\sum_{j=1}^{N}(a_j^\dagger a_j - b_j^\dagger b_j), \tag{1}$$

where δ and $i\gamma$ are the distortion factor with a unit tunneling constant and the alternating imaginary potential magnitude, respectively. Here $a_l^\dagger$ and $b_l^\dagger$ are the creation operator of the particle at the lth site in A and B sublattices. The particle can be a fermion or a boson, depending on their own commutation relations. In the second term, two kinds of summation can be taken, corresponding to open and periodic boundary conditions. For nonzero γ, it is still a $\mathcal{PT}$-symmetry system. Here, the time-reversal operation $\mathcal{T}$ is such that $\mathcal{T}i\mathcal{T} = -i$, while the effect of parity is such that $\mathcal{P}a_l\mathcal{P} = b_{N+1-l}$ and $\mathcal{P}b_l\mathcal{P} = a_{N+1-l}$. Applying operators $\mathcal{P}$ and $\mathcal{T}$ on the Hamiltonian (1), one has $[\mathcal{T}, H] \neq 0$ and $[\mathcal{P}, H] \neq 0$, but

$$[\mathcal{PT}, H] = 0. \tag{2}$$

In parallel, H also has chiral-time symmetry

$$\{\mathcal{CT}, H\} = 0, \tag{3}$$

where operator $\mathcal{C}$ is defined as

$$\mathcal{C}a_j\mathcal{C}^{-1} = a_j, \quad \mathcal{C}b_j\mathcal{C}^{-1} = -b_j. \tag{4}$$

The situation here is a little different from the case associated with $\mathcal{PT}$ symmetry. In quantum mechanics, we say that a Hamiltonian H has symmetry represented by an operator $\mathcal{L}$ if $[H, \mathcal{L}] = 0$. The word "symmetry" is also used in a different sense in condensed-matter physics. We say that a system with Hamiltonian H has chiral symmetry if $\{H, \mathcal{C}\} = 0$. The physics of $\mathcal{C}$ depends on the model discussed [57–62]. A non-Hermitian system with $\mathcal{CT}$ symmetry has been systematically studied in Ref. [63].

According to the non-Hermitian quantum theory, such a Hamiltonian may have a fully real spectrum within a certain parameter region. The boundary of the region is the critical point of a quantum phase transition associated with $\mathcal{PT}$-symmetry breaking. For the system with a periodic boundary condition, the critical point occurs at $\gamma = \gamma_c = 2\delta$, which is also referred as to the EP [55]. The exact solution is obtained in the strong dimerization limit, which shows that the equal-level-spacing high-frequency standing-wave modes (EHSM) [56] can be achieved in a chain system when the corresponding ring system is tuned at the EP, as depicted schematically in Fig. 1. According to Ref. [56], in the strong dimerization limit $1+\delta \gg 1-\delta$, the Hamiltonian

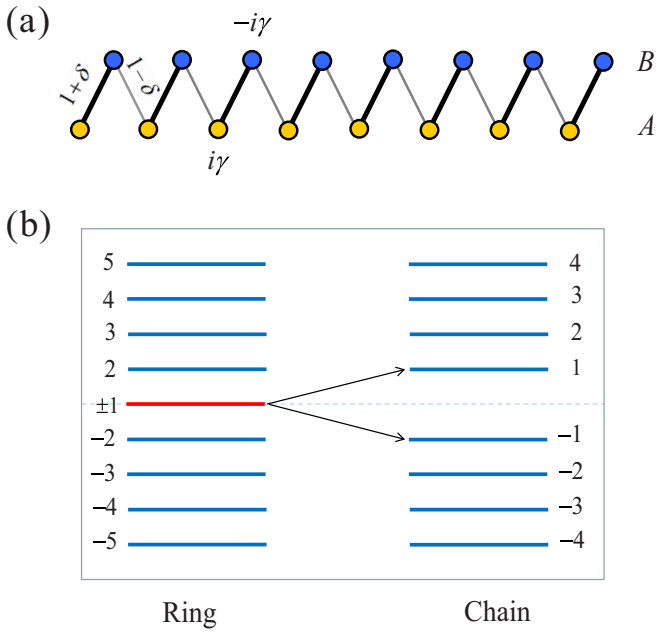

FIG. 1. (a) Schematic for the 1D non-Hermitian SSH model. It consists of two sublattice, A (golden) and B (blue). Black thick and gray thin lines indicate the hopping between two nearest-neighbor sites with amplitudes $(1+\delta)$ and $(1-\delta)$, respectively. Two sublattices have opposite site imaginary potentials $\pm i\gamma$, representing the physical gain and loss. It has $\mathcal{PT}$ symmetry and it can have a full real spectrum in the case of $1 > \delta > 0$ and $\gamma < \gamma_c$ (see the text). (b) The spectra of the non-Hermitian SSH model at $\gamma = \gamma_c$ with periodic and open boundary (by breaking one of the weak hopping term) conditions, respectively. In both cases, energy levels near zero are equally spaced. For a ring system, zero-level coalescence is split into two levels when the open boundary condition is imposed.

with an open boundary condition can be diagonalized approximately, and the single-particle eigenvectors for $\gamma = \gamma_c$ can be expressed as

$$|\psi_n^\pm\rangle = \sqrt{\frac{\pm(-1)^N}{N+1}}\sum_{j=1}^{N}(-1)^j \sin(kj) \times (e^{\pm i\varphi_k/2}a_j^\dagger \pm e^{\mp i\varphi_k/2}b_j^\dagger)|0\rangle, \tag{5}$$

where k is defined as

$$k = \frac{n\pi}{N+1}, \quad n \in [1, N]. \tag{6}$$

The corresponding eigenenergy is

$$\varepsilon_k = \sqrt{[(1+\delta) - (1-\delta)\cos k]^2 - \gamma_c^2} \tag{7}$$

and

$$\tan\varphi_k = \frac{\gamma_c}{\varepsilon_k}. \tag{8}$$

We note that γ_c is no longer the EP for the open chain, and we find that the energy levels can be expressed as

$$E_n^{\pm} = \pm n\omega,\ \omega = \frac{\sqrt{2\delta(1-\delta)}\pi}{N+1}, \tag{9}$$

approximately for small n, which satisfy $n < n_c = (N/\pi)\sqrt{|0.48\delta/(3-5\delta)|}$ (see the Appendix). $|\psi_n^{\pm}\rangle$ is normalized in the framework of the Dirac inner product, i.e., $\langle\psi_m^{\pm}|\psi_n^{\pm}\rangle = \delta_{mn}$. It indicates that the spectrum ε_k consists of two branches separated by an energy gap $\Delta = 2\omega$, which ensures the existence of the equal-level-spacing standing-wave modes (ESM) around zero energy. In this model, the value of γ_c is necessary for achieving a set of eigenstates as ESM, which is crucial for the construction of our target state. In addition, the deliberate expression of the set of eigenvectors $\{|\psi_n^{\pm}\rangle\}$ satisfies

$$\mathcal{PT}|\psi_n^{\pm}\rangle = (-1)^n|\psi_n^{\pm}\rangle \tag{10}$$

and

$$\mathcal{CT}|\psi_n^{\pm}\rangle = -i|\psi_n^{\mp}\rangle, \tag{11}$$

which will be used to analyze the dynamics of the system in the following sections.

III. LASING DYNAMICS

In this section, we will investigate the dynamics for a class of a specific state. We focus on the initial state satisfying three conditions: (i) The Dirac probability distribution is localized in the coordinate space, (ii) the superposition coefficient of the wave function is nonvanishing only for small n, and (iii) it has CT symmetry. It is expected that such kinds of initial state may possess lasing dynamics due to the following reasons: Although the non-Hermitian SSH chain does not have an EP at γ_c, its corresponding ring system has an EP at zero energy. However, a local wave packet does not know whether the boundary condition is open or periodic unless its final state touches the boundary. Then the wave packet should partially exhibit the EP dynamics, which obeys the time evolution in a Jordan block [53,54,64] when the initial state $|\psi(0)\rangle$ has a component of the coalescing eigenstates of the SSH ring at the EP. On the other hand, the above condition (ii) ensures that $|\psi(0)\rangle$ probably contains such a coalescing component. From the analysis of the last section, conditions of (ii) and (iii) constrain the evolved state to possess symmetric probability distribution and time-reflection symmetry, which make the dynamics more convenient to describe.

Before focusing on specific initial states, we study some features of time evolution for an initial state satisfying the above condition (ii). For small n, we have

$$|\psi(m\tau)\rangle = \sum_{n=1,\sigma=\pm} c_n^{\sigma}\exp(-i2nm\sigma\pi)\big|\psi_n^{\sigma}\big\rangle = |\psi(0)\rangle, \tag{12}$$

where

$$\tau = \frac{2\pi}{\omega} = \frac{2(N+1)}{\sqrt{2\delta(1-\delta)}}, \tag{13}$$

and m is an integer. This indicates that the initial state $|\psi(m\tau)\rangle$ reappears periodically with period τ. This property is not a direct result of the symmetry of the system. In addition, for the present model, we have

$$\left|\psi\left[\left(m+\frac{1}{2}\right)\tau\right]\right\rangle = \sum_{n=1,\sigma=\pm} c_n^{\sigma}\exp(-in\sigma\pi)\big|\psi_n^{\sigma}\big\rangle = \sum_{n=1,\sigma=\pm} c_n^{\sigma}\mathcal{PT}\big|\psi_n^{\sigma}\big\rangle, \tag{14}$$

based on Eq. (10). Specifically, for a class of initial states with a set of real (or total imaginary) $\{c_n^{\sigma}\}$, we have

$$\left|\psi\left[\left(m+\frac{1}{2}\right)\tau\right]\right\rangle = \mathcal{PT}|\psi(0)\rangle, \tag{15}$$

i.e., such states reappear periodically at the symmetric position with period $\tau/2$ [40]. On the other hand, the dynamics of a Jordan block should exhibit increasing probability with a power law [53,54,64]. The combination of the two results gives us the following statement. In general, the probability should experience both increasing and decreasing processes within the time scale $\tau/2$. This agrees with the prediction of dynamics with time-reflection symmetry.

Now we construct a class of initial states that meet the above three conditions. We will show that such states exhibit lasing dynamics during the time evolution. The initial state has the form

$$c_n^{\sigma} = \sigma\Lambda\sin(n\kappa_0)\frac{\exp(-qn)}{n}, \tag{16}$$

where Λ is a normalization constant, $q \geqslant 0$, and $\kappa_0 \in (0,\pi)$ are related to the shape and position of the initial state, respectively. Obviously, c_n^{σ} is real and vanishing for large n. We note that the initial state

$$|\psi(0)\rangle = \Lambda\sum_{n=1,\sigma=\pm}^{N}\sigma\sin(n\kappa_0)\frac{\exp(-qn)}{n}\big|\psi_n^{\sigma}\big\rangle \tag{17}$$

has both $\mathcal{PT}$ and $\mathcal{CT}$ symmetries for the case with $\kappa_0 = \pi/2$. To demonstrate the localization of $|\psi(0)\rangle$ in the coordinate space, we plot the profile of $|\psi(0)\rangle$ with several typical κ_0 in Fig. 2. This indicates that $|\psi(0)\rangle$ is a local wave packet with the center position $2N(\kappa_0/\pi)$. The time evolution of such a local initial state is independent of the initial position within a certain time scale. Then we can focus on the state $|\psi(0)\rangle$ with $\kappa_0 = \pi/2$. The evolved state always has a symmetric profile in real space. Such symmetric dynamics is convenient

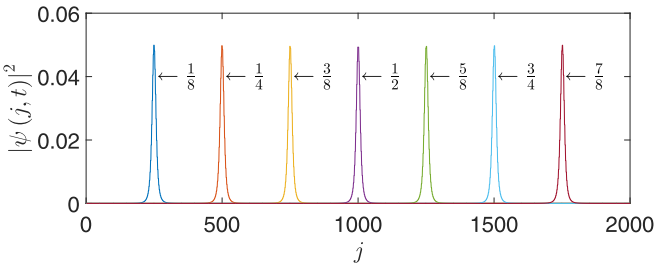

FIG. 2. Profiles of initial states from the plot of Eq. (17) with $\kappa_0 = \pi/8,\ \pi/4,\ldots,7\pi/8$, respectively. This shows that the initial states are all localized with the identical shape in coordinate space, and the central position is the linear function of κ_0. The parameters are $2N = 2000,\ \delta = 0.9,\ \gamma = 1.8$, and $q = 0.02$.

for analytical analysis, and the obtained result can be applied to the case with $\kappa_0 \neq \pi/2$ by a simple translation due to the locality of the evolved state.

To estimate the profile of the evolved state, we derive the evolved wave vector in the following compact form:

$$|\psi(t)\rangle \approx \Lambda_N \sum_{j=1}^{N} \sum_{\rho,\upsilon,\eta=\pm 1} \arctan\left(\frac{\sin\theta}{e^q - \cos\theta}\right) \times (-1)^j \rho\upsilon\eta e^{i\eta\pi/4} \left|2j - \frac{1}{2}(1-\eta)\right\rangle, \quad (18)$$

where $\Lambda_N = \frac{\Lambda}{2}\sqrt{(-1)^N/(N+1)}$ and

$$\theta = \rho\kappa_0 + \frac{\upsilon\pi j}{N+1} + \omega t - \frac{\eta}{4\delta}. \quad (19)$$

In Fig. 3, the profiles of $|\langle l|\psi(t)\rangle|^2$ are plotted, which are obtained by numerical simulations and approximate analytical expression in Eq. (18). It shows that the evolved state is a flat-top wave packet with uniformly increasing width. After bouncing from the two ends of the chain, it turns back to the initial state and starts the next cycling. This observation can be explained by the following analysis for a special case.

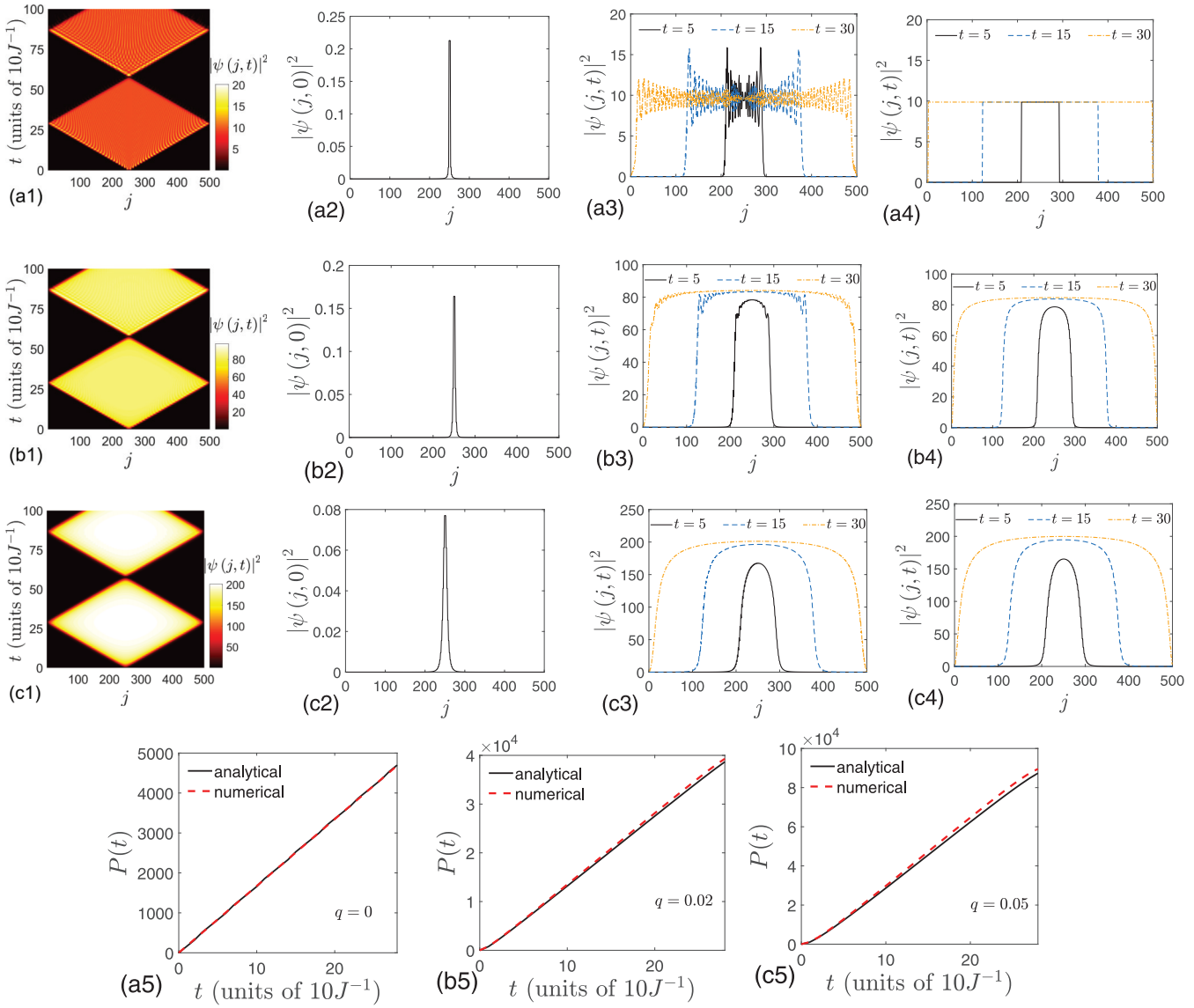

FIG. 3. Profiles of evolved wave packets for initial states expressed in Eq. (17) with $\kappa_0 = \pi/2$ and several typical q values. $q = 0$ for (a1,a2,a3,a4), $q = 0.02$ for (b1,b2,b3,b4), and $q = 0.05$ for (c1,c2,c3,c4). (a1,b1,c1) Three-dimensional plots of evolved states for initial states plotted in (a2,b2,c2) obtained by numerical simulations. (a2,b2,c2) Plots of initial states from Eq. (17). (a3,b3,c3) Profiles of evolved states at several instants obtained by numerical simulations. (a4,b4,c4) The same as (a3,b3,c3) but obtained by analytical expression in Eq. (18). (a5,b5,c5) Plots of the Dirac norm $P(t)$ obtained by numerical simulations (dash line) and analytical expression (solid line) for different q, (a5) for $q = 0$, (b5) for $q = 0.02$, and (c5) for $q = 0.05$. The parameters for the SSH chain are $2N = 500$, $\delta = 0.9$, and $\gamma = 1.8$. The time is in units of $10J^{-1}$, where J is the scale of the Hamiltonian and we take $J = 1$. The analytical expressions agree well with the numerical results, especially for nonzero q. This shows that the evolved states are flat-top (rectangular shape for zero q) with uniformly increasing width, exhibiting stationary lasing dynamics before touching the boundary.

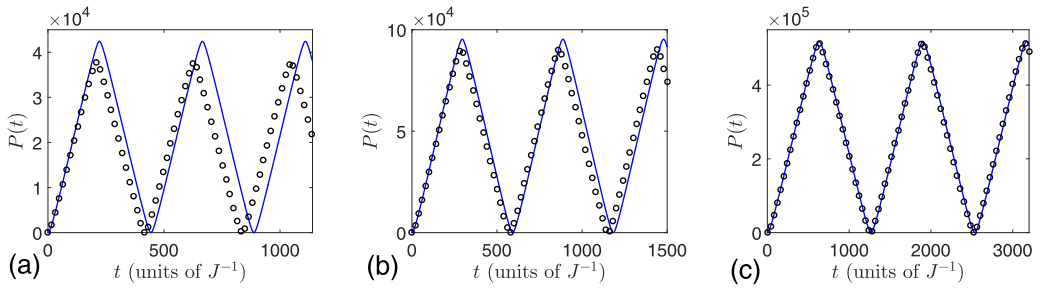

FIG. 4. Plots of $P(t)$ obtained by numerical simulations (empty circle) and analytical expression (solid line) in Eq. (22). The parameters for the SSH chain are $2N = 500$, $\gamma = 2\delta$, and (a) $\delta = 0.8$, (b) $\delta = 0.9$, and (c) $\delta = 0.98$, respectively. The initial states are taken in the form in Eq. (17) with $\kappa_0 = \pi/2$ and $q = 0.05$. It shows that $P(t)$ is a triangle wave with period $\tau = 2(N+1)/\sqrt{2\delta(1-\delta)}$. The analytical expressions agree well with the numerical results, especially for the cases with strong dimerization.

When $q = 0$, the expression of the evolved state reduces to

$$|\psi(t)\rangle \approx \frac{\Lambda_N}{2}\sum_{j=1}^{N}\sum_{\rho,\upsilon,\eta=\pm1}(-1)^j\rho\upsilon\eta e^{i\eta\pi/4}r(\theta) \times\left|2j-\frac{1}{2}(1-\eta)\right\rangle, \tag{20}$$

where $r(\theta)$ is a periodic triangular function defined as

$$r(\theta) = (\pi-\theta)/2 + n\pi, \quad \theta\in[0,2\pi)+2\pi n, \tag{21}$$

with $n \in Z$.

For $\kappa_0 = \pi/2$, the Dirac norm of the evolved state is

$$\begin{aligned}P(t) &= \langle\psi(t)|\psi(t)\rangle \\ &\approx -\frac{\Lambda^2 e^{-2q}}{2}\mathrm{Re}\left[e^{-i2\omega t}\Phi\left(e^{-4(q+i\omega t)},2,\frac{1}{2}\right)\right] \\ &\quad +\Lambda^2\sum_{\sigma=\pm}\sigma\mathrm{Li}_2(\sigma e^{-2q}),\end{aligned} \tag{22}$$

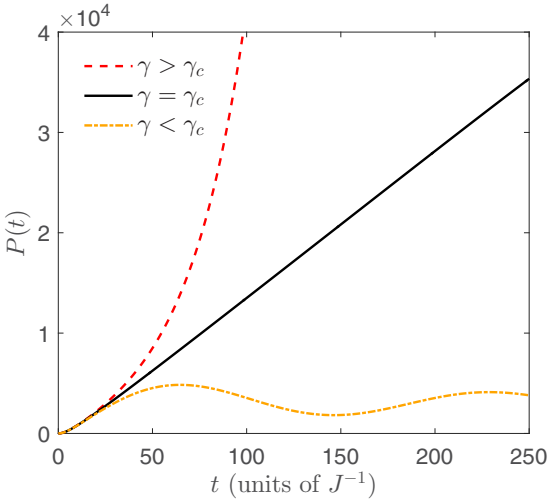

FIG. 5. Plots of $P(t)$ obtained by numerical simulations for three typical values of γ. The parameters for the SSH chain are $2N = 500$, $\delta = 0.9$, and $\gamma_c = 1.8$. The initial states are taken in the form in Eq. (17) with $\kappa_0 = \pi/2$ and $q = 0.02$. We can see that $P(t)$ is exponential for $\gamma > \gamma_c$, linear for $\gamma = \gamma_c$, and oscillates for $\gamma < \gamma_c$, respectively. It indicates that $\gamma = \gamma_c$ serves as the threshold of the active laser medium.

where $\Phi(z,s,\alpha) = \sum_{n=0}^{\infty} z^n/(n+\alpha)^s$ is the Lerch transcendental function and $\mathrm{Li}_n(z) = \sum_{k=1}^{\infty} z^k/k^n$ is the polylogarithm function. In particular, taking $q = 0$, the Dirac norm $P(t)$ becomes a triangular wave

$$P(t) \approx \frac{2\Lambda^2\pi^2}{\tau}\begin{cases} t - n\tau/2, & t\in[0,\tau/4)+n\tau/2, \\ -t+(n+1)\tau/2, & t\in[\tau/4,\tau/2)+n\tau/2, \end{cases} \tag{23}$$

with $n \in Z$. As expected, it is the direct results of the uniform expanding flat-top wave packet. We also plot the function $P(t)$ from Eq. (22) and numerical simulation for several typical values of δ in Fig. 4, which indicates that our analytical result agrees well with the numerical result, especially for strong dimerization.

Obviously, such a stationary solution is related to the condition $\gamma = \gamma_c$. It is natural to ask what happens when γ deviates from γ_c. To answer this question, numerical simulations are performed by exact diagonalization. We plot the total probability as a function of time for three cases in Fig. 5. It shows that the plot is exponential, linear, and oscillates for $\gamma > \gamma_c$, $\gamma = \gamma_c$, and $\gamma < \gamma_c$, respectively. It indicates that γ_c is the threshold for the lasing medium.

It is presumable that the lasing dynamics is independent of the position of the initial state if the chain is large enough. It differs from the lasing mechanics based on the SS in a non-Hermitian scattering center, in which only the scattering center acts as the active lasing medium. The underlying mechanism is the translational symmetry and the existence of EP in the bulk region of the chain.

IV. INITIAL GAUSSIAN WAVE PACKET

What we have done so far is to show analytically the existence of the stable laser mode. However, it does not mean that one has to stimulate a laser by such a specific initial state. In principle, any initial state $|\Phi(0)\rangle$ satisfying $\langle\Phi(0)|\psi(0)\rangle \neq 0$ and the remaining component of state $|\Phi(0)\rangle - \langle\psi(0)|\Phi(0)\rangle|\psi(0)\rangle$ is not amplified so much, and $|\Phi(0)\rangle$ should have a similar effect to the deliberately designed $|\psi(0)\rangle$ in Eq. (17).

In practice, a Gaussian wave packet is a good candidate as an initial state. It is a local state, but it can represent a plane wave when its width becomes large enough. Another reason we choose the Gaussian wave packet is that the profile of the

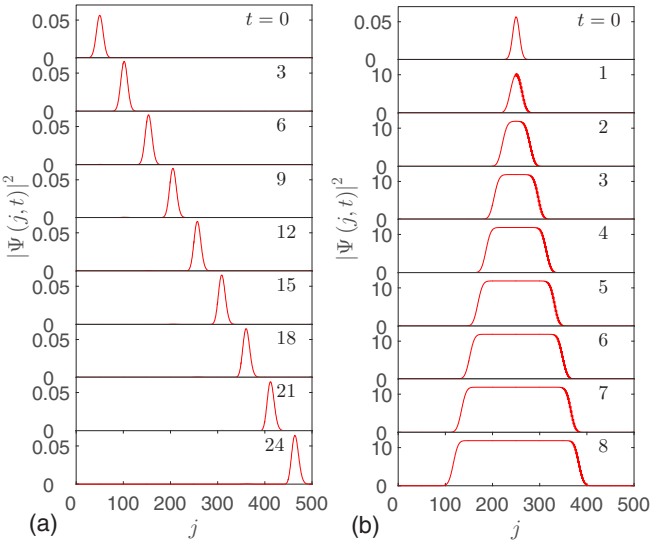

FIG. 6. Plots of profiles of the evolved states for initial state Eq. (24) at several typical instants obtained by numerical simulations (a) for $k_c = -\pi/2$, $\alpha = 0.1$, $N_c = 450$ and (b) for $k_c = \pi/2$, $\alpha = 0.1$, $N_c = 250$. The parameters for the SSH chain are $2N = 500$, $\delta = 0.5$, and $\gamma = 1$. The time is in units of $10J^{-1}$. It indicates that the predesigned initial state can be replaced by a Gaussian wave packet to trigger a stationary laser state.

predesigned initial state plotted in Fig. 2 is very close to a Gaussian wave packet. In other words, a wave packet probably contains the component of the state $|\psi(0)\rangle$ in Eq. (17). An initial Gaussian wave packet reads

$$|\Psi(j,0)\rangle = \Omega^{-1/2} e^{-\alpha^2 (j-N_c)^2/2} e^{ik_c j} |j\rangle, \tag{24}$$

where N_c is the Gaussian wave center, k_c is the central vector, and $\Omega = \sqrt{\pi}/\alpha$ is the normalization factor. Factor Ω ensures that the Dirac probability of the initial state is unity. In the previous works [49,50], such an initial state is employed to stimulate the laser emission from the non-Hermitian scattering center. In the present model, it is easy to check that $\langle\Psi(j,0)|\psi(0)\rangle \neq 0$ for $k_c = \pi/2$ and $\langle\Psi(j,0)|\psi(0)\rangle = 0$ for $k_c = -\pi/2$. The numerical simulation results are presented in Fig. 6.

To demonstrate the similar dynamical behavior of two lasing mechanics, we consider a system that couples two semi-infinite chains: one is the non-Hermitian SSH chain, and the other is a Hermitian uniform chain. The Hamiltonian reads

$$H_{CP} = \sum_{j=0}^{\infty} [1 + (-1)^j \delta] a_j^\dagger a_{j+1} + (1-\delta) \sum_{j=0}^{-\infty} a_j^\dagger a_{j-1} + \text{H.c.} - i\gamma \sum_{j=0}^{\infty} (-1)^j a_j^\dagger a_j, \tag{25}$$

where $\gamma = \gamma_c = 2\delta$. A detailed investigation of this model is not the aim of the present paper. Here we only present the numerical simulation results (Fig. 7) for the dynamics of an initial Gaussian wave packet Eq. (24). It indicates that

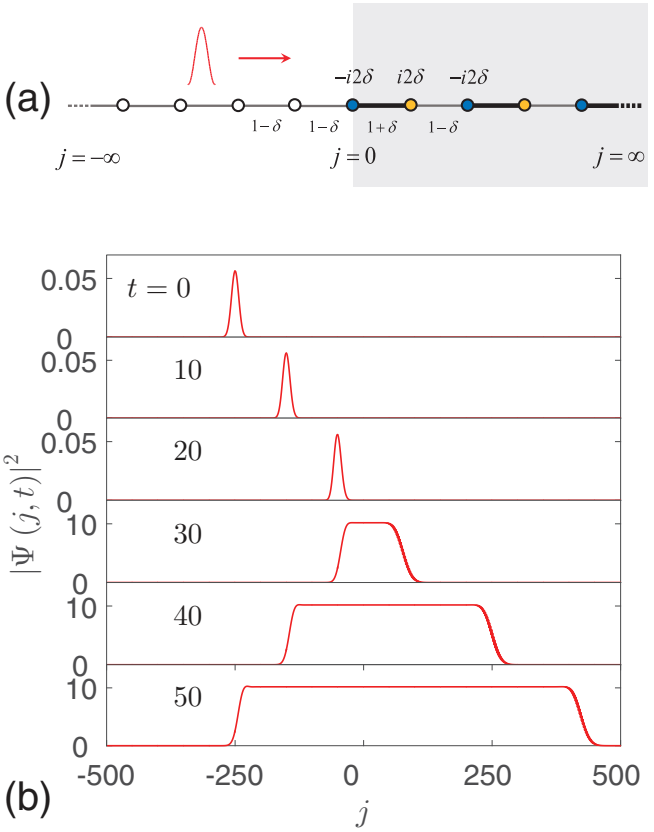

FIG. 7. (a) Schematic for the system in Eq. (25). It couples two semi-infinite chains: one is a Hermitian uniform chain, while the other is the non-Hermitian SSH chain. (b) Plots of profiles of the evolved state for initial state Eq. (24) in Hamiltonian Eq. (25) at several typical instants obtained by numerical simulations. We take $k_c = -\pi/2$, $\alpha = 0.1$, $N_c = -250$, $\delta = 0.5$, and $\gamma = 1$. The time is in units of $10J^{-1}$. It indicates that a stationary laser state can be triggered in a non-Hermitian system and transports in a Hermitian system.

the boundary acts as a non-Hermitian scattering center in association with the SS dynamics.

V. PROBABILITY PRESERVING AND ELASTIC COLLISION

From the analysis in the above sections, we find that the extending rectangular wave or flat-top wave packet bounds back at two ends of the chain. We note that there are two features in the reflection process: (i) There is no interference pattern (standing wave) as usual. (ii) This process acts like a time-refection one, i.e., the profiles of input and output are identical. In this section, we will study the underlying mechanism of this phenomenon. For this purpose, it will be convenient to think in terms of the symmetric case and extend the conclusion to a general case, i.e., taking the case with $\kappa_0 = \pi/2$. In this case, the initial state is a superposition of eigenstates with small odd n. These eigenstates are all long-wavelength standing waves, the superposition of which has no ability to form an interference pattern with small frequency.

On the one hand, Fig. 3 and an analytical analysis show that two edges of the flat-top wave packet touch the two ends

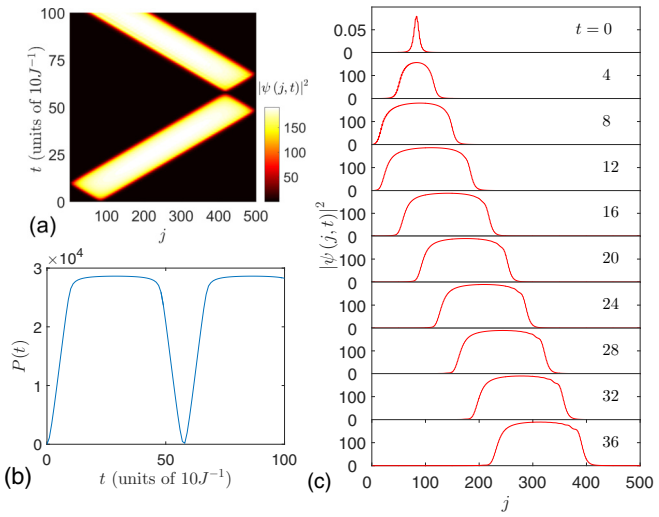

FIG. 8. (a) Three-dimensional plots of evolved wave packets for initial states expressed in Eq. (17) with $\kappa_0 = \pi/6$ and $q = 0.05$, obtained by numerical simulation. (b) Plot of $P(t)$ for the time evolutions for (a). (c) The profiles of the evolved wave packet at several typical instants. The parameters for the SSH chain are $2N = 500$, $\delta = 0.9$, and $\gamma = 1.8$. It shows that the evolved states become a traveling wave packet after the first reflection on the one side, i.e., it propagates as a translational motion, preserving the probability before the subsequent reflection on the other side.

of the chain at instant $t = \tau/4$. We note that

$$|\psi(\tau/4)\rangle = \sum_{n=1,\sigma=\pm} c^{\sigma}_{2n-1} \exp(-in\sigma\pi) i\sigma \left|\psi^{\sigma}_{2n-1}\right\rangle, \tag{26}$$

which are both $\mathcal{PT}$- and $\mathcal{CT}$-symmetric, satisfying

$$\mathcal{PT}|\psi(\tau/4)\rangle = |\psi(\tau/4)\rangle, \tag{27}$$

$$\mathcal{CT}|\psi(\tau/4)\rangle = i|\psi(\tau/4)\rangle, \tag{28}$$

taking $|\psi(\tau/4)\rangle$ as an initial state, and using the conclusion [Eq. (A21)] in the Appendix, we obtain

$$|\langle j|\psi(\tau/4 + \Delta t)\rangle|^2 \approx |\langle j|\psi(\tau/4 - \Delta t)\rangle|^2, \tag{29}$$

i.e., the reflection process is symmetric about the instant $t = \tau/4$. We refer to this phenomenon as elastic reflection due to the fact that it is analogous to a mass-spring system in classical physics.

On the other hand, the dynamics before reflection is the same for an initial state located anywhere in the chain. Then the elastic reflection also happens for the initial state with $\kappa_0 \neq \pi/2$. We will show that the combination of two such features leads to a probability preserving dynamics that usually appears in a Hermitian system. Such a process occurs when an initial state is located far from the center of the chain. As an extension of the wave packet, one of its edges moves in the opposite direction after the elastic bounce from one end of the chain. Then two edges of the wave packet move in the same direction with the same speed, which results in a translational motion of the wave packet, preserving the Dirac probability. Figure 8 displays a profile of the evolved state for an initial state with $\kappa_0 \neq \pi/2$.

Now we consider the time evolution for an initial state as a superposition of two wave packets. Such an investigation is trivial for a Hermitian system. However, some unexpected phenomena may be found in a non-Hermitian system, although it is also a linear system. This is because the

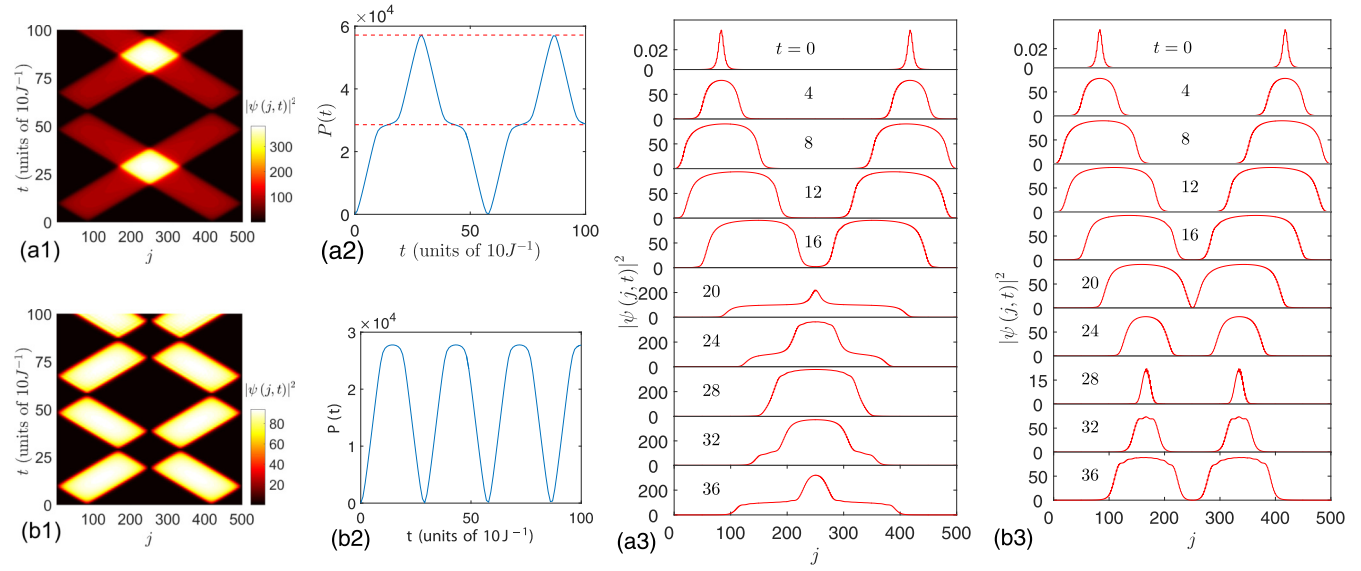

FIG. 9. The same as that in Fig. 8, but for initial states (a1) $|\Psi_+\rangle$ and (b1) $|\Psi-\rangle$ expressed in Eq. (30) with $\kappa_{01} = \pi/6$, $\kappa_{02} = 5\pi/6$, obtained by numerical simulation. Parts (a2) and (b2) are plots of $P(t)$ for the time evolutions for (a1) and (b1), respectively. Parts (a3) and (b3) are the profiles of the evolved wave packets at several typical instants for (a1) and (b1), respectively. We see that when two wave packets are separated, the total probability is always constant, while it changes when they overlap. In the case of (a2), the probability doubles as indicated by two dotted lines. It is due to the anomalous interference phenomenon, in which there are no interference patterns. In contrast, from (b2) we see that the probability becomes very small, as if two wave packets annihilate together or absorb each other. It is a peculiar dynamics, with no counterpart in a Hermitian system.

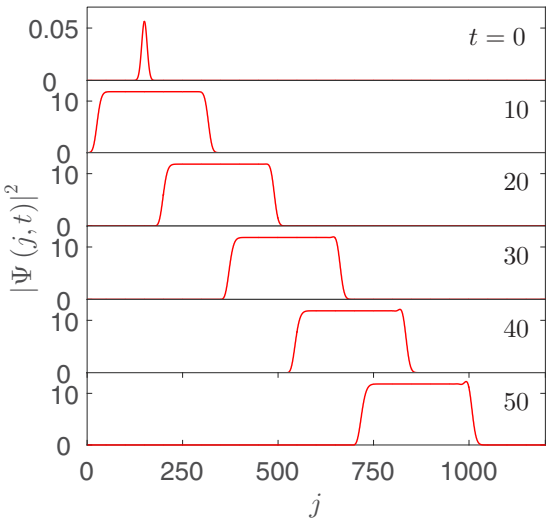

FIG. 10. Plots of profiles of the evolved states for initial state Eq. (24) in a semi-infinite non-Hermitian SSH chain at several typical instants. The parameters for numerical simulations are $k_c = \pi/2$, $\alpha = 0.1$, $N_c = 150$, $\delta = 0.5$, and $\gamma = 1$. The time is in units of $10J^{-1}$. It indicates that the predesigned initial state can be replaced by a Gaussian wave packet to generate a laser wave train with a length on demand.

Dirac probability is not defined by a canonical inner product (biorthonormal inner product). The initial state is taken in the form

$$|\Psi_{\pm}\rangle = \frac{\Lambda}{\sqrt{2}} \sum_{n=1,\sigma=\pm} \sigma[\sin(n\kappa_{01}) \pm \sin(n\kappa_{02})] \times \frac{\exp(-qn)}{n} |\psi_n^{\sigma}\rangle, \tag{30}$$

where κ_{01} and κ_{02} determine the initial locations of two wave packets. The trajectories and profiles of two wave packets are clear when they do not overlap. We are interested in what happens when they meet. To answer this question, we employ the numerical simulation to compute the probability of the evolved state. Figure 9 shows that the dynamics of $|\Psi_+\rangle$ behaves as a Hermitian one, while $|\Psi_-\rangle$ exhibits a peculiar behavior: It looks like two wave packets cancel each other out when they meet. Furthermore, Fig. 10 indicates that the predesigned initial state can be replaced by a Gaussian wave packet to generate a laser wave train with a length on demand.

VI. SUMMARY

In summary, we have investigated the non-Hermitian analog of an active laser medium, and we found a scenario for the mechanism of lasing in the framework of quantum mechanics. We have proposed an alternative lasing mechanism induced by the EP in a finite non-Hermitian system rather than SS in an infinite system with a non-Hermitian scattering center. The key difference between two mechanisms is that a laser can be fired everywhere on the former while only at the scattering center in the latter. The present non-Hermitian system also exhibits many peculiar dynamic behaviors, such as elastic reflection, collision, and probability preserving translational propagation, etc. The underlying mechanism of such features is the balance of distortion and staggered imaginary potentials, while an SS laser solution does not require the balance. In general, the positions of EPs are a little different for the same model but with different boundary conditions, or more generally speaking, with and without some defects. When the initial state is local in coordinate space, its dynamics within a certain period of time is independent of the boundary condition and its initial location. This provides a way to explore the dynamics, which is a combination of a quasi-Hermitian and Jordan block time evolution in a general non-Hermitian system. So the key point in practice is the specific class of initial states. For the present model, the linear increase of probability arises from such a combination. It can be seen from the nonzero overlap

$$|\langle\phi_c|\psi(0)\rangle| \approx \frac{\sqrt{\delta(1-\delta)}\Lambda}{N\delta} \arctan\left(\frac{\sin\kappa_0}{\sinh q}\right), \tag{31}$$

where

$$|\phi_c\rangle = \frac{1}{\sqrt{2N}} \sum_{j=1}^{N} (-1)^j (|2j-1\rangle + i|2j\rangle) \tag{32}$$

is the coalescing eigenvector of the conjugate Hamiltonian $H^{\dagger}$ in Eq. (1) with the periodic boundary condition. Our results, on the one hand, provide an alternative lasing theory in the context of non-Hermitian quantum mechanics, and on the other hand they indicate that the non-Hermitian system is fertile ground for many unknown features in physics.

ACKNOWLEDGMENT

This work was supported by National Natural Science Foundation of China (under Grant No. 11874225).

APPENDIX

1. Definition of "small n"

From the dispersion relation in Eq. (7) we have the approximate expression of energy around k_0 as

$$\varepsilon_k \approx \varepsilon_{k_0} + \left(\frac{\partial\varepsilon_k}{\partial k}\right)_{k_0} (k-k_0) + \frac{1}{2}\left(\frac{\partial^2\varepsilon_k}{\partial k^2}\right)_{k_0} \times (k-k_0)^2 + \frac{1}{3!}\left(\frac{\partial^3\varepsilon_k}{\partial k^3}\right)_{k_0} (k-k_0)^2 + \cdots. \tag{A1}$$

If $\gamma = \gamma_c = 2\delta$, we have

$$\left(\frac{\partial\varepsilon_k}{\partial k}\right)_{0^+} = \sqrt{2(1-\delta)\delta}, \tag{A2}$$

$$\left(\frac{\partial^2\varepsilon_k}{\partial k^2}\right)_{0} = 0, \tag{A3}$$

$$\left(\frac{\partial^3\varepsilon_k}{\partial k^3}\right)_{0^+} = \frac{(3-5\delta)\sqrt{(1-\delta)\delta}}{4\sqrt{2}\delta}. \tag{A4}$$

For a non-Hermitian SSH system at EP, there exists a critical n_c that denotes the critical number of energy levels. Any levels with $n < n_c$ are quasi-equal-level spacing. The value of n_c can be estimated as follows. The ratio between

the contributions from linear and cubic terms can be utilized to characterize the precision of the equal-level spacing. For example, we can take

$$\left|\lim_{k\to 0^+}\frac{\frac{1}{3!}\left(\frac{\partial^3\varepsilon_k}{\partial k^3}\right)_{\gamma=\gamma_c}k_c^3}{\left(\frac{\partial\varepsilon_k}{\partial k}\right)_{\gamma=\gamma_c}k_c}\right|=0.01 \tag{A5}$$

to determine n_c by

$$k_c\approx\frac{n_c\pi}{N}. \tag{A6}$$

With a certain approximation, one can define

$$n_c=\frac{N}{\pi}\sqrt{\left|\frac{0.48\delta}{3-5\delta}\right|}. \tag{A7}$$

The result shows that the value of n_c is a function of the size of the system N and the distortion factor δ. Then we can define "small n," which satisfies $n<n_c=\frac{N}{\pi}\sqrt{|\frac{0.48\delta}{3-5\delta}|}$.

2. Symmetry of the initial state

In this subsection, we show why the initial state is constructed in that way. We start with some general properties of dynamics for a $\mathcal{PT}$- and $\mathcal{CT}$-symmetric system, which is helpful for the subsequent discussions. In Secs. III and V, we reveal two features of dynamics, which are related to the symmetries of the system, but not exact results. The first one is a quasisymmetric time evolution, and the second one is about time-reflection symmetry. The obtained result in this subsection is applicable for a more general system.

Unlike the symmetry related to a linear operator $\mathcal{L}$, here $\mathcal{PT}$ and $\mathcal{CT}$ are antilinear operators, which act in a different way in the time evolution for a symmetric initial state. Consider a Hamiltonian $\mathcal{H}$ with $\mathcal{L}$, $\mathcal{PT}$, and $\mathcal{CT}$ symmetries, i.e.,

$$[\mathcal{L},\mathcal{H}]=[\mathcal{PT},\mathcal{H}]=\{\mathcal{CT},\mathcal{H}\}=0, \tag{A8}$$

respectively. An initial state $|\psi(0)\rangle$ is taken as the eigenstate of $\mathcal{L}$, $\mathcal{PT}$, and $\mathcal{CT}$, e.g.,

$$\mathcal{L}|\psi(0)\rangle=\mathcal{PT}|\psi(0)\rangle=\mathcal{CT}|\psi(0)\rangle=|\psi(0)\rangle. \tag{A9}$$

We are interested in the symmetry of the evolved state $|\psi(t)\rangle=e^{-i\mathcal{H}t}|\psi(0)\rangle$. Direct derivations show that

$$\mathcal{L}|\psi(t)\rangle=\mathcal{CT}|\psi(t)\rangle=|\psi(t)\rangle, \tag{A10}$$

$$\mathcal{PT}|\psi(t)\rangle=|\psi(-t)\rangle, \tag{A11}$$

which indicate that the evolved state may not maintain the initial symmetry associated with an antilinear operator.

Applying the above analysis to the present SSH model, we can make the following observations. Here $\mathcal{L}$ can be taken as an operator $\sum_{j=1}^{N}(a_j^\dagger a_j+b_j^\dagger b_j)$ as an example, which obeys Eq. (A10). For the $\mathcal{PT}$-symmetric initial state, we have the symmetric Dirac probability distribution

$$\begin{aligned}|\langle j|\psi(0)\rangle|^2&=|\langle j|\mathcal{PT}|\psi(0)\rangle|^2\\&=|\langle 2N+1-j|\psi(0)\rangle|^2.\end{aligned} \tag{A12}$$

However, for the evolved state we have

$$\begin{aligned}|\langle j|\psi(t)\rangle|^2&=|\langle j|(\mathcal{PT})^{-1}e^{iHt}\mathcal{PT}|\psi(0)\rangle|^2\\&=|\langle 2N+1-j|\psi(-t)\rangle|^2,\end{aligned} \tag{A13}$$

which cannot guarantee a symmetric probability profile.

Now we will show that the time evolution is approximately symmetric for a class of initial state. For small n, the approximate eigenstate of the Hamiltonian with even N reads

$$\begin{aligned}|\psi_n^\pm\rangle\approx e^{\pm i\pi/4}\sqrt{\frac{\pm1}{N+1}}\sum_{j=1}^{N}(-1)^j\sin(kj)\\\times(a_j^\dagger-ib_j^\dagger)|0\rangle\end{aligned} \tag{A14}$$

by taking

$$\varphi_k\approx\frac{\pi}{2}. \tag{A15}$$

The implication of the approximation is clearly that two eigenstates $|\psi_n^\pm\rangle$ with opposite energy $\pm E_n$ have the same expression. The time evolution of $|\psi_n^\pm\rangle$ is

$$\begin{aligned}e^{-iHt}|\psi_n^\pm\rangle\approx e^{\mp iE_nt}e^{\pm i\pi/4}\sqrt{\frac{\pm1}{N+1}}\sum_{j=1}^{N}(-1)^j\\\times\sin(kj)(a_j^\dagger-ib_j^\dagger)|0\rangle.\end{aligned} \tag{A16}$$

Furthermore, for a $\mathcal{CT}$-symmetric state, e.g.,

$$|\varphi_+\rangle=\sum_n c_n^+(|\psi_n^+\rangle+|\psi_n^-\rangle), \tag{A17}$$

with real c_n^+, we have

$$\begin{aligned}e^{-iHt}|\varphi_+\rangle&=\sum_{n=1}c_n^+(e^{-iE_nt}|\psi_n^+\rangle+e^{iE_nt}|\psi_n^-\rangle)\\&\approx\sqrt{\frac{1}{N+1}}\sum_{j=1}^{N}f(j,t)(a_j^\dagger-ib_j^\dagger)|0\rangle,\end{aligned} \tag{A18}$$

where

$$f(j,t)=\sum_n(-1)^jc_n^+(e^{-iE_nt}e^{i\pi/4}+i\,\text{c.c.})\sin(kj). \tag{A19}$$

The function $\sin(kj)$ is an odd (even) function about the center of the chain when n is even (odd). If the $|\varphi_+\rangle$ is a $\mathcal{PT}$-symmetric state, the summation in $f(j,t)$ runs over even (or odd) n only. The function $f(j,t)$ is also symmetric due to the fact that any combination of odd (even) functions is also an odd (even) function. Then probability $|\langle 0|(a_j+ib_j)e^{-iHt}|\varphi_+\rangle|^2$ is a symmetric function, i.e.,

$$|\langle j|\psi(t)\rangle|^2\approx|\langle 2N+1-j|\psi(t)\rangle|^2. \tag{A20}$$

Together with Eq. (A13), we have

$$|\langle j|\psi(t)\rangle|^2\approx|\langle j|\psi(-t)\rangle|^2, \tag{A21}$$

which indicates that the time evolution has time-reflection symmetry about zero t.

We conclude that the evolved state has symmetric probability distribution and time-reflection symmetry if the initial state satisfies three conditions: (i) $\mathcal{PT}$ symmetry, (ii) $\mathcal{CT}$ symmetry, and (iii) involving very small n. We would like to point out that these results are approximate rather than exact, and they are referred as to quasisymmetric dynamics. This result is important to construct and characterize the laser mode in the present non-Hermitian SSH chain.

[1] T. Gao, E. Estrecho, K. Y. Bliokh, T. C. H. Liew, M. D. Fraser, S. Brodbeck, M. Kamp, C. Schneider, S. Höfling, Y. Yamamoto, F. Nori, Y. S. Kivshar, A. G. Truscott, R. G. Dall, and E. A. Ostrovskaya, Observation of non-Hermitian degeneracies in a chaotic exciton-polariton billiard, Nature (London) **526**, 15522 (2015).

[2] H. Lü, S. K. Özdemir, L. M. Kuang, F. Nori, and H. Jing, Exceptional Points in Random-Defect Phonon Lasers, Phys. Rev. Appl. **8**, 044020 (2017).

[3] J. Zhang, B. Peng, Ş. K. Özdemir, K. Pichler, D. O. Krimer, G. Zhao, F. Nori, Y. Liu, S. Rotter, and L. Yang, A phonon laser operating at an exceptional point, Nat. Photon. **12**, 479 (2018).

[4] C. M. Bender and S. Boettcher, Real Spectra in Non-Hermitian Hamiltonians Having PT Symmetry, Phys. Rev. Lett. **80**, 5243 (1998).

[5] C. M. Bender, S. Boettcher, and P. N. Meisinger, PT-symmetric quantum mechanics, J. Math. Phys. **40**, 2201 (1999).

[6] P. Dorey, C. Dunning, and R. Tateo, Supersymmetry and the spontaneous breakdown of PT symmetry, J. Phys. A **34**, L391 (2001).

[7] P. Dorey, C. Dunning, and R. Tateo, Spectral equivalences, Bethe ansatz equations, and reality properties in PT-symmetric quantum mechanics, J. Phys. A **34**, 5679 (2001).

[8] C. M. Bender, D. C. Brody, and H. F. Jones, Complex Extension of Quantum Mechanics, Phys. Rev. Lett. **89**, 270401 (2002).

[9] A. Mostafazadeh, Pseudo-Hermiticity versus PT-symmetry III: Equivalence of pseudo-Hermiticity and the presence of antilinear symmetries, J. Math. Phys. **43**, 3944 (2002).

[10] A. Mostafazadeh, Exact PT-symmetry is equivalent to hermiticity, J. Phys. A **36**, 7081 (2003).

[11] H. F. Jones, On pseudo-Hermitian Hamiltonians and their Hermitian counterparts, J. Phys. A **38**, 1741 (2005).

[12] M. Znojil, Tridiagonal-symmetric N-by-N Hamiltonians and a fine-tuning of their observability domains in the strongly non-Hermitian regime, J. Phys. A **40**, 13131 (2007).

[13] M. Znojil, Discrete-symmetric models of scattering, J. Phys. A **41**, 292002 (2008).

[14] M. Znojil, Gegenbauer-solvable quantum chain model, Phys. Rev. A **82**, 052113 (2010).

[15] H. Jing, S. K. Özdemir, X. Y. Lü, J. Zhang, L. Yang, and F. Nori, PT-Symmetric Phonon Laser, Phys. Rev. Lett. **113**, 053604 (2014).

[16] D. Leykam, K. Y. Bliokh, C. Huang, Y. D. Chong, and F. Nori, Edge Modes, Degeneracies, and Topological Numbers in Non-Hermitian Systems, Phys. Rev. Lett. **118**, 040401 (2017).

[17] Z. Gong, Y. Ashida, K. Kawabata, K. Takasan, S. Higashikawa, and M. Ueda, Topological Phases of Non-Hermitian Systems, Phys. Rev. X **8**, 031079 (2018).

[18] T. Liu, Y. R. Zhang, Q. Ai, Z. Gong, K. Kawabata, M. Ueda, and F. Nori, Second-Order Topological Phases in Non-Hermitian Systems, Phys. Rev. Lett. **122**, 076801 (2019).

[19] K. Y. Bliokh, D. Leykam, M. Lein, and F. Nori, Topological non-Hermitian origin of surface Maxwell waves, Nat. Commun. **10**, 580 (2019).

[20] A. Guo, G. J. Salamo, D. Duchesne, R. Morandotti, M. Volatier-Ravat, V. Aimez, G. A. Siviloglou, and D. N. Christodoulides, Observation of PT-Symmetry Breaking in Complex Optical Potentials, Phys. Rev. Lett. **103**, 093902 (2009).

[21] C. E. Rüter, K. G. Makris, R. El-Ganainy, D. N. Christodoulides, M. Segev, and D. Kip, Observation of parity-time symmetry in optics, Nat. Phys. **6**, 192 (2010).

[22] W. Wan, Y. Chong, L. Ge, H. Noh, A. D. Stone, and H. Cao, Time-reversed lasing and interferometric control of absorption, Science **331**, 889 (2011).

[23] Y. Sun, W. Tan, H.-Q. Li, J. Li, and H. Chen, Experimental Demonstration of a Coherent Perfect Absorber with PT Phase Transition, Phys. Rev. Lett. **112**, 143903 (2014).

[24] L. Feng, Y. L. Xu, W. S. Fegadolli, M. H. Lu, J. E. B. Oliveira, V. R. Almeida, Y. F. Chen, and A. Scherer, Experimental demonstration of a unidirectional reflectionless parity-time metamaterial at optical frequencies, Nat. Mater. **12**, 108 (2013).

[25] B. Peng, Ş. K. Özdemir, F. Lei, F. Monifi, M. Gianfreda, G. L. Long, S. Fan, F. Nori, C. M. Bender, and L. Yang, Parity-time-symmetric whispering-gallery microcavities, Nat. Phys. **10**, 394 (2014).

[26] L. Chang, X. Jiang, S. Hua, C. Yang, J. Wen, L. Jiang, G. Li, G. Wang, and M. Xiao, Parity-time symmetry and variable optical isolation in active-passive-coupled microresonators, Nat. Photon. **8**, 524 (2014).

[27] L. Feng, Z. J. Wong, R. M. Ma, Y. Wang, and X. Zhang, Single-mode laser by parity-time symmetry breaking, Science **346**, 972 (2014).

[28] H. Hodaei, M. A. Miri, M. Heinrich, D. N. Christodoulides, and M. Khajavikhan, Parity-time–symmetric microring lasers, Science **346**, 975 (2014).

[29] M. Wimmer, A. Regensburger, M. A. Miri, C. Bersch, D. N. Christodoulides, and U. Peschel, Observation of optical solitons in PT-symmetric lattices, Nat. Commun. **6**, 7782 (2015).

[30] W. D. Heiss, The physics of exceptional points, J. Phys. A **45**, 444016 (2012).

[31] I. Rotter, A non-Hermitian Hamilton operator and the physics of open quantum systems, J. Phys. A **42**, 153001 (2009).

[32] I. Rotter and A. F. Sadreev, Avoided level crossings, diabolic points, and branch points in the complex plane in an open double quantum dot, Phys. Rev. E **71**, 036227 (2005).

[33] H. Xu, D. Mason, L. Jiang, and J. G. E. Harris, Topological energy transfer in an optomechanical system with exceptional points, Nature (London) **537**, 80 (2016).

[34] B. F. Samsonov, Spectral singularities of non-Hermitian Hamiltonians and SUSY transformations, J. Phys. A **38**, 571 (2005).

[35] A. A. Andrianov, F. Cannata, and A. V. Sokolov, Spectral singularities for non-Hermitian one-dimensional Hamiltonians:

puzzles with resolution of identity, J. Math. Phys. **51**, 052104 (2010).
[36] A. Mostafazadeh, Spectral Singularities of Complex Scattering Potentials and Infinite Reflection and Transmission Coefficients at Real Energies, Phys. Rev. Lett. **102**, 220402 (2009).
[37] S. Longhi, Spectral singularities in a non-Hermitian Friedrichs-Fano-Anderson model, Phys. Rev. B **80**, 165125 (2009).
[38] S. Longhi, Spectral singularities and Bragg scattering in complex crystals, Phys. Rev. A **81**, 022102 (2010).
[39] A. Mostafazadeh, Optical spectral singularities as threshold resonances, Phys. Rev. A **83**, 045801 (2011).
[40] X. Z. Zhang, L. Jin, and Z. Song, Perfect state transfer in PT-symmetric non-Hermitian networks, Phys. Rev. A **85**, 012106 (2012).
[41] J. G. Muga, J. P. Palaob, B. Navarroa, and I. L. Egusquizac, Complex absorbing potentials, Phys. Rep. **395**, 357 (2004).
[42] K. G. Makris, R. El-Ganainy, D. N. Christodoulides, and Z. H. Musslimani, Beam Dynamics in PT Symmetric Optical Lattices, Phys. Rev. Lett. **100**, 103904 (2008).
[43] Z. H. Musslimani, K. G. Makris, R. El-Ganainy, and D. N. Christodoulides, Optical Solitons in PT Periodic Potentials, Phys. Rev. Lett. **100**, 030402 (2008).
[44] Z. Lin, A. Pick, M. Loncar, and A. W. Rodriguez, Enhanced Spontaneous Emission at Third-Order Dirac Exceptional Points in Inverse-Designed Photonic Crystals, Phys. Rev. Lett. **117**, 107402 (2016).
[45] J. Wiersig, Sensors operating at exceptional points: General theory, Phys. Rev. A **93**, 033809 (2016).
[46] Y. L. Liu, R. B. Wu, J. Zhang, S. K. Özdemir, L. Yang, F. Nori, and Y. X. Liu, Controllable optical response by modifying the gain and loss of a mechanical resonator and cavity mode in an optomechanical system, Phys. Rev. A **95**, 013843 (2017).
[47] X. Z. Zhang, L. Tian, and Y. Li, Optomechanical transistor with mechanical gain, Phys. Rev. A **97**, 043818 (2018).
[48] Z. Ahmed, Zero width resonance (spectral singularity) in a complex PT-symmetric potential, J. Phys. A **42**, 472005 (2009).
[49] C. Li, L. Jin, and Z. Song, Non-Hermitian interferometer: Unidirectional amplification without distortion, Phys. Rev. A **95**, 022125 (2017).
[50] P. Wang, S. Lin, L. Jin, and Z. Song, Parallel dynamics between non-Hermitian and Hermitian systems, Phys. Rev. A **97**, 062101 (2018).
[51] H. Ramezani, H.-K. Li, Y. Wang, and X. Zhang, Unidirectional Spectral Singularities, Phys. Rev. Lett. **113**, 263905 (2014).
[52] X. M. Yang, X. Z. Zhang, C. Li, and Z. Song, Dynamical signature of the moiré pattern in a non-Hermitian ladder, Phys. Rev. B **98**, 085306 (2018).
[53] E. M. Graefe, H. J. Korsch, and A. E. Niederle, Mean-Field Dynamics of a Non-Hermitian Bose-Hubbard Dimer, Phys. Rev. Lett. **101**, 150408 (2008).
[54] H. Cartarius and N. Moiseyev, Fingerprints of exceptional points in the survival probability of resonances in atomic spectra, Phys. Rev. A **84**, 013419 (2011).
[55] W. H. Hu, L. Jin, Y. Li, and Z. Song, Probability-preserving evolution in a non-Hermitian two-band model, Phys. Rev. A **86**, 042110 (2012).
[56] K. L. Zhang, P. Wang, G. Zhang, and Z. Song, Simple harmonic oscillation in a non-Hermitian Su-Schrieffer-Heeger chain at the exceptional point, Phys. Rev. A **98**, 022128 (2018).
[57] J. K. Asbóth, L. Oroszlány, and A. Pályi, A short course on topological insulators, Lect. Notes Phys. **919**, 10 (2016).
[58] S. Malzard, C. Poli, and H. Schomerus, Topologically Protected Defect States in Open Photonic Systems with Non-Hermitian Charge-Conjugation and Parity-Time Symmetry, Phys. Rev. Lett. **115**, 200402 (2015).
[59] H. Guo and S. Chen, Kaleidoscope of symmetry-protected topological phases in one-dimensional periodically modulated lattices, Phys. Rev. B **91**, 041402(R) (2015).
[60] L. Li and S. Chen, Characterization of topological phase transitions via topological properties of transition points, Phys. Rev. B **92**, 085118 (2015).
[61] P. Peng, W. Cao, C. Shen, W. Qu, J. Wen, L. Jiang, and Y. Xiao, Anti-parity–time symmetry with flying atoms, Nat. Phys. **12**, 1139 (2016).
[62] T. E. Lee, Anomalous Edge State in a Non-Hermitian Lattice, Phys. Rev. Lett. **116**, 133903 (2016).
[63] S. Lin and Z. Song, Wide-range-tunable Dirac-cone band structure in a chiral-time-symmetric non-Hermitian system, Phys. Rev. A **96**, 052121 (2017).
[64] E. M. Graefe, H. J. Korsch, and A. E. Niederle, Quantum-classical correspondence for a non-Hermitian Bose-Hubbard dimer, Phys. Rev. A **82**, 013629 (2010).